Applied Catalysis B: Environmental 138–139 (2013) 381–390

Contents lists available at SciVerse ScienceDirect

Applied Catalysis B: Environmental

journal homepage: www.elsevier.com/locate/apcatb

Effects of β-cyclodextrin introduction to zirconia supported-cobalt oxide catalysts: From molecule-ion associations to complete oxidation of formaldehyde

Lei Bai[a,b,d], Frédéric Wyrwalski[a,b,d], Jean-François Lamonier[a,c,d], Andrei Y. Khodakov[a,c,d], Eric Monflier[a,b,d], Anne Ponchel[a,b,d,*]

[a] Univ Lille Nord de France, F-59000 Lille, France
[b] UArtois, UCCS, Faculté des Sciences Jean Perrin, Rue Jean Souvraz, SP-18, F-62300 Lens, France
[c] USTL, UCCS, F-59650 Villeneuve d'Ascq, France
[d] CNRS, UMR 8181, France

ARTICLE INFO

Article history:
Received 27 October 2012
Received in revised form 1 March 2013
Accepted 5 March 2013
Available online 18 March 2013

Keywords:
Cobalt catalysts
Cobalt precursor
Catalyst preparation
Cyclodextrins
VOC oxidation

ABSTRACT

The present paper deals with the impact of the addition of β-cyclodextrin on the genesis of cobalt active phases in zirconia-supported catalysts and on their performances in the complete oxidation of formaldehyde. With this aim, a series of cobalt catalysts supported on zirconia (5 wt.%) is prepared by wet impregnation using mixtures of $Co(NO_3)_2$ and β-cyclodextrin as precursors. After the impregnation step, the materials are dried and calcined under air at 400 °C. Different ratios of β-cyclodextrin to cobalt have been employed to obtain insight in the role of β-cyclodextrin, i.e. from 0.01 to 1. The ability of β-cyclodextrin to interact with the cobalt salt is investigated in solution by UV–vis spectroscopy, ion conductivity in water and dynamic light scattering measurements. After the impregnation step, the cobalt supported materials are characterized at different stages of the preparation (before and after calcination) by means of conventional techniques including UV–vis spectroscopy, thermogravimetry, N_2 adsorption/desorption, X-ray diffraction and temperature-programmed reduction analysis. Characterization results suggest that the carbohydrate ligand bound to the cobalt species retards the decomposition of the cobalt complexes into Co_3O_4. Finally, these cobalt oxide catalysts prepared from β-cyclodextrin are able to catalyze the oxidation of formaldehyde more efficiently than the control sample. The results are explained in terms of cobalt oxide dispersion and cobalt-support interactions. Indeed, the cobalt oxide particles generated by the thermal decomposition of β-cyclodextrin-Co(II) adducts are on the one hand smaller than those formed with cobalt nitrate alone and on the other hand reducible at lower temperatures, two key factors in the catalytic oxidation reactions.

1. Introduction

Volatile organic compounds (VOCs) are recognized as major contributors to air pollution through their toxic and carcinogenic human health effects and cause noxious effects on the impacts on the global environmental system, particularly a high ozone potential depletion [1].

According to the Göteborg protocol, the maximum VOC emission level by 2010 in the EU member countries had to be reduced by 40% as compared to the base year 1990 [2] and the protocol is currently being reviewed with a view to setting new ceilings to be achieved by 2020. Various methods have been developed to reduce or eliminate the VOCs emissions. For instance, uses of porous materials such as activated carbons or zeolites are well-established methods to minimize the pollutant level [3], however these adsorption techniques only transfer the containments to another phase. One effective method is the conversion of VOC to carbon dioxide and water via catalytic oxidation. Advantages of this technology are low fuel consumption, particularly with the proper choice of heat exchanger and no formation of partial oxidation products, such as carbon monoxide.

The catalysts conventionally used for the oxidation of VOCs are generally divided into two classes. The first one is the supported noble metal catalysts, commonly employing platinum, palladium, rhodium or gold as active phases. As recently reported in several articles or reviews [4–6], noble metal catalysts usually show superior catalytic performances in relatively low temperatures ranges.

* Corresponding author at: UArtois, UCCS, Faculté des Sciences Jean Perrin, Rue Jean Souvraz, SP-18, F-62300 Lens, 7 France. Tel.: +33 0 321791754.
E-mail address: anne.ponchel@univ-artois.fr (A. Ponchel).

0926-3373/$ – see front matter © 2013 Elsevier B.V. All rights reserved.
http://dx.doi.org/10.1016/j.apcatb.2013.03.015

However, the high cost and limited availability of noble metals might be a hindrance to their development. The second one is the transition metal oxide materials, which offer a low cost alternative to the first group, when they are designed as catalysts [7]. A number of transition metal oxides and their combinations have been reported for their effectiveness in catalytic oxidation, including for example, Ce-Zr mixed oxides, perovskites, copper, manganese and cobalt oxide-based catalysts [8–17].

In particular, Co_3O_4 catalysts (bulk or supported) have received considerable attention for a long time [14], finding applications in a variety of oxidative reactions, such as low-temperature carbon monoxide oxidation [16–18], ammonia oxidation [19] and VOCs oxidation [20]. However, in order to achieve comparable levels of activities to those produced by the noble metal counterparts, higher reaction temperatures and higher amounts of active phase are generally required (at least 5 wt.%). In this context, for the design of efficient cobalt oxide-based catalysts with high activity and selectivity, it is important to optimize the dispersion and size of the metal oxide crystallites and control their redox properties, especially those related to Co(III)/Co(II), which is assumed to be the active redox couple in catalytic oxidation [21]. Indeed, the reducibility of the active cobalt species is a crucial parameter. It is generally accepted that the reaction mechanism of oxidation of hydrocarbons is a redox type mechanism, in which the key steps are the supply of active oxygen species by the readily reducible oxide and its re-oxidation by molecular oxygen [22,23]. These factors, i.e. dispersion, size and reducibility, may depend on the preparation method, nature of the cobalt precursor and on the interactions between the cobalt species and support.

Conventional cobalt oxide-based catalysts are generally prepared by aqueous impregnation of porous oxide supports with a solution of cobalt nitrate, followed by calcination under air at high temperatures. Previous reports have shown that the performances of supported cobalt catalysts can be improved by promotion with transition metal oxide, such as MnO_x [24] or by the controlled addition of organic compounds to the impregnating solution. Thus, the use of ethylenediaminetetraacetic (EDTA) [25–27] and ethylenediamine [28–31] has been extensively investigated to produce smaller cobalt particles. This effect is usually associated to the strong ability of the amino compounds to chelate cobalt ions and form well-defined coordination complex, therefore leading to better dispersions of the surface active cobalt species after calcination. However, the main drawback of the N-ligands lies in the fact that the stability of the cobalt complexes is sensitive to pH changes, therefore requiring stringent conditions of synthesis. Although focused on the cobalt-based catalysts in the Fischer-Tropsch synthesis, it has also been established that the addition of carbohydrate compounds during catalyst impregnation could have a beneficial impact on the dispersion of cobalt sites and on their overall catalytic performances. Thus, the possibility of using sucrose [32], sorbitol [33,34] to promote of silica- and alumina-supported cobalt catalysts was successfully reported. However, the utilization of carbohydrate compounds cannot be easily generalized. Indeed, antagonist effects on cobalt reducibility have been reported as a function of the nature of the inorganic support, which affects the total number of cobalt active sites and consequently the catalytic activities.

Recently, β-cyclodextrins (water-soluble cyclic oligosaccharides formed of 7 glucopyranose units; Scheme 1) have emerged as potential tools for the preparation of metal or metal oxide materials [35–38]. Indeed, these polyhydroxylated compounds are well-known for their ability to stabilize host–guest complexes [39,40], metallic nanoparticles [41–43] and molecule-ion adducts with inorganic metal salts [44–46]. In particular, our group has expanded the scope of the use of cyclodextrins to the preparation of alumina-supported cobalt catalysts for the Fischer-Tropsch synthesis [47]. Beneficial effects on the reaction rates were observed, as a result of enhancement of the cobalt dispersions and increase in the concentration of crystallite nucleation sites. Though this latter work has opened new opportunities in the field of the design of transition metal oxide supported catalysts, efforts have to be made in the near future to expand the use of cyclodextrins to prepare nano-supported catalysts via impregnation, with high activity, selectivity and stability. The objectives imply to have a better understanding in the role of cyclodextrins at each stage of the preparation, starting from the interactions occurring between the cyclodextrin and metal precursor in the aqueous phase, up to the genesis of the active phase in the catalyst.

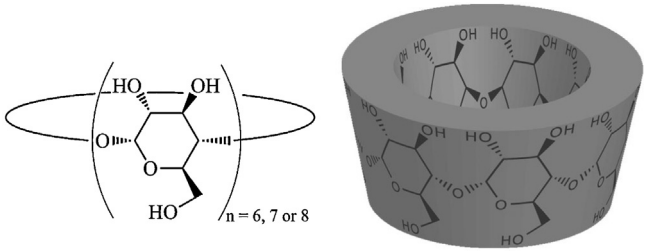

Scheme 1. Chemical representations of the native cyclodextrins.

In line with this, we have decided to examine in a thorough manner the impact of β-cyclodextrin (β-CD) on the synthesis of new zirconia-supported cobalt oxide catalysts employed in the VOC oxidation. Zirconia is selected as the support because of its good mechanical properties, high thermal stabilities and chemical inertness to cobalt oxides compared to SiO_2 or Al_2O_3 [48]. Briefly, a series of catalysts containing 5 wt.% cobalt is prepared by wet impregnation, starting from mixtures of cobalt nitrate and β-CD of variable ratios as precursors. After the impregnation step, the materials are dried and calcined under air at 400 °C for 4 h. The ability of β-CD to design efficient supported cobalt oxide catalysts is discussed on the basis of physicochemical data collected at different points of the preparation (solution, dried state and calcined state) via UV–vis spectroscopy, ion conductivity in water, dynamic light scattering, thermogravimetry, N_2 adsorption/desorption, X-ray diffraction and temperature-programmed reduction. Finally, the catalytic performances are examined in the total oxidation of VOC. Formaldehyde (HCHO) has been chosen as the probe molecule because HCHO emitted from buildings, furnishings and decorative materials is becoming an important pollutant of indoor and outdoor air with established negative effects on human health [49].

2. Experimental

2.1. Catalyst preparation

The starting zirconia has been prepared according to a precipitation procedure previously reported in the literature [28], and in our experimental conditions, the as-prepared zirconia has a BJH mean pore size of 6.6 nm and a specific surface area of 62.6 $m^2\,g^{-1}$.

Cobalt oxide catalysts, with a theoretical cobalt content of 5 wt.%, were synthesized by impregnation using aqueous solutions of cobalt nitrate and β-CD as follows: in a round bottom flask, 0.520 g (0.179 mmol) of cobalt (II) nitrate hexahydrate (Sigma–Aldrich, ACS reagent, >98% purity) was added to 150 mL of an aqueous solution containing x equivalent of native β-CD ($C_{42}H_{70}O_{35}$, M = 1134 g mol^{-1} Roquette Frères, Lestrem, France). The solution was kept under constant stirring for 2 h at ambient temperature. The support (2 g) was then added to the mixed cobalt solution and the solid suspension was stirred for 2 supplementary hours. Water was slowly removed in a rotary evaporator at 60 °C until dryness. The recovered solid was dried overnight in an oven

Table 1
Elemental analysis, specific surface area and H_2-TPR data of the zirconia supported-cobalt catalysts.

Sample	β-CD/Co ratio	Co (wt.%)[a]	S_{BET} ($m^2\,g^{-1}$) dried solid	S_{BET} ($m^2\,g^{-1}$) calcined solid	H_2 consumption ($\mu mol\,g^{-1}$)		Percentage of H_2 consumption (%)[d]	Reduction temperature $Co^{3+} \rightarrow Co^{2+}$ (°C)[e]
					Theoretical[b]	Experimental[c]		
ZrO_2	–	0	–	62.6	0	0	–	–
Co(N)/Zr	0	4.8	50.2	56.6	1080	1094	23%	344
Co-$CD_{0.01}$/Zr	0.01	4.7	22.1	57.3	1064	1062	22%	338
Co-$CD_{0.05}$/Zr	0.05	4.8	22.6	58.5	1080	1104	23%	316
Co-$CD_{0.1}$/Zr	0.1	4.7	21.7	56.3	1053	1070	22%	230 (shoulder), 317
Co-$CD_{0.2}$/Zr	0.2	4.6	22.3	58.4	1032	1007	22%	230 (shoulder), 318
Co-CD_1/Zr	1.0	4.5	11.7	61.2	1015	1028	22%	345

[a] Determined by elemental analysis.
[b] Theoretical consumption estimated by considering the total conversion of Co_3O_4 to zerovalent cobalt according to the following equation: $Co_3O_4 + 4H_2 \rightarrow 3Co + 4H_2O$.
[c] Experimental consumption estimated by integration of the area under the H_2-TPR signal from room temperature to 800 °C using Autochem II 2920 software.
[d] Percentage of H_2 consumption estimated by integration of the area in the low-temperature region under the H_2-TPR signal using Autochem II 2920 software.
[e] Measured at the peak maxima in the low-temperature region in the H_2-TPR profile.

at 100 °C and calcined at 400 °C for 4 h. (heating rate of 2 °C min^{-1}) in a flow of air (2 L h^{-1}). The so-obtained catalysts are denoted as Co-CD_x/Zr where x corresponds to the initial molar ratio of cobalt to cyclodextrin, with x = 0.01, 0.05, 0.1, 0.2 and 1. The control zirconia-supported catalyst prepared with the same procedure, but without addition of β-CD, is designated as Co(N)/Zr. Note that the cobalt content in the catalysts has been determined by elemental analysis at the Service Central d'Analyse du CNRS (Vernaison, France). As shown in Table 1, the resulting values vary between 4.5 and 4.8 wt.% Co depending on the sample.

2.2. Methods of characterization

Dynamic light scattering (DLS) studies were conducted in aqueous solutions of β-CD alone or in a mixture with cobalt nitrate at a controlled temperature (25 ± 0.1 °C) using a Malvern Zetasizer Nano ZS equipment. The Zetasizer Nano ZS apparatus uses a 632.8 nm helium-neon laser and analyses the scattered light at an angle of 173° by utilizing a non-invasive backscatter technique. The samples were prepared at the desired concentration and were kept under vigorous stirring during 2 h before analysis. Then, the samples were filtered through a sterile 0.22 μm filter. A total of 20 scans, each with a period of 50 s, was accumulated for each sample. All samples were analyzed in triplicate using the DTS Software from Malvern Instruments to acquire the correlogram (correlation function versus time).

UV–vis spectrophotometric analysis in the transmission mode was carried out with a Lambda 19 PerkinElmer spectrophotometer.

Ion conductivity experiments were conducted in aqueous solutions at a controlled temperature (25 °C) in a jacketed glass reactor (250 mL) using a CDM210 MeterLab instrument from Radiometer as apparatus.

Nitrogen adsorption/desorption isotherms were obtained at −196 °C by using a Nova 2200 apparatus from Quantachrome Corporation, after having degassed the sample under vacuum overnight at 100 °C. The specific area was calculated from the Brunauer–Emmett–Teller (BET) equation using P/P_0 values in the 0.05–0.25 range and the pore size distribution was obtained from the desorption branch using the Barrett–Joyner–Halenda (BJH) method.

Thermogravimetric measurements (TG) were performed using a TA Instruments SDT 2960 instrument equipped with a flow gas system. The solid was treated from room temperature to 800 °C (5 °C min^{-1}) under a gas mixture composed of helium (80 vol.%) and oxygen (20 vol.%) with a flow of 75 mL min^{-1}. Approximately, 10 mg of sample was heated in an open platinum crucible. In addition, the temperature-programmed decomposition products were analyzed on-line with a Pfeiffer vacuum Omnistar GSD 320 mass spectrometer. Only selected gases evolved were measured, such as CO_2, H_2O and NO.

The structure of the calcined samples was analyzed by X-ray diffraction (XRD). Experiments were conducted on a Bruker D8 Advance diffractometer in Bragg-Brentano geometry equipped with a copper anode (λ = 1.5418 Å) and a 1D PSD Lynxeye detector. The scattering intensities were measured over an angular range of $10° < 2\theta < 80°$ for all the samples with a step-size of $\Delta(2\theta) = 0.02°$. The diffraction patterns have been indexed by comparison with the Joint Committee on Powder Diffraction Standards (JCPDS) files.

Temperature-programmed reduction (H_2-TPR) profiles of samples were recorded using a Micromeritics AutoChem 2920 chemisorption analyzer. Accurate amounts of calcined sample (0.150 g) were purged in a flow of pure argon at 200 °C for 1 h to remove traces of water (heating rate 10 °C min^{-1}). After cooling to 30 °C, H_2-TPR experiments were performed using a 5% H_2/Ar mixture at a flow rate of 10 mL min^{-1}. The sample was heated from 30 °C to 1000 °C using a heating rate of 10 °C min^{-1} and the H_2 consumption was detected by a thermal conductivity detector (TCD). Knowing that the TPR profiles, such as the peak shape and maximum temperature, are sensitive to the experimental conditions, appropriate selections of operating conditions [amount of reducible species (S_0), carrier flow rate (F), hydrogen concentration (C_0) and heating rate (β)] are required to maintain a good resolution in the TPR profiles. According to the literature data, two characteristic parameters have been defined: (i) $k = S_0/(F \times C_0)$, which should be kept in the range of 55–140 s with heating rates between 6 and 18 K min^{-1} [50,51] and (ii) $p = (\beta \times S_0)/(F \times C_0)$, which should be kept as low as possible (typically less than 20 °C) [50,52]. The established experimental conditions lead to acceptable values of k and p values, 113 s and 19 °C respectively.

2.3. Catalytic activity test

The formaldehyde catalytic oxidation was performed in a fixed bed micro-reactor (i.d. 10 mm) loaded with 200 mg of catalyst. The reaction mixture containing 150 ppm HCOH, 20 vol.% O_2 was balanced by He and the flow rate was fixed at 100 mL min^{-1}. The reaction temperature was increased from room temperature to 250 °C with a fixed heating rate of 1 °C min^{-1}. The effluent gas from the reactor containing formaldehyde, oxygen, carbon dioxide or carbon monoxide was analyzed on-line by a Varian CP 4900 MicroGC chromatograph equipped with a thermal conductivity detector. Each catalytic run was performed in duplicate and the reported results are the average between the two runs.

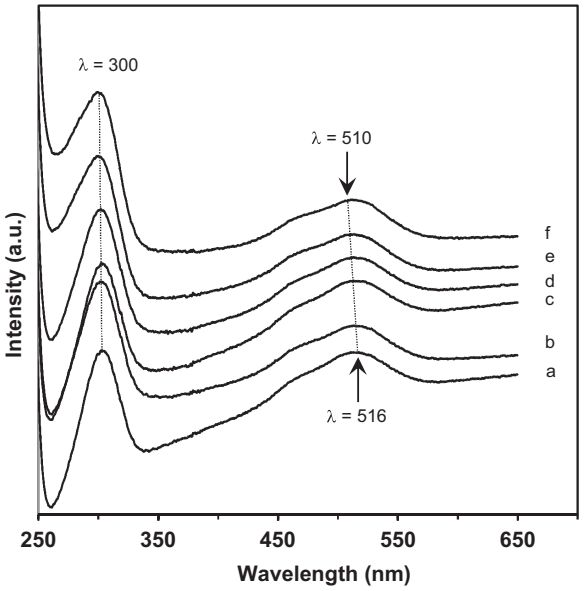

Fig. 1. Absorption UV–vis spectra of aqueous solutions of $Co(NO_3)_2$ at different β-CD concentrations: 0 (a), 2 (b), 4 (c), 6 (d), 8 (e) and 10 (f) mM. [$Co(NO_3)_2$] = 1 mM.

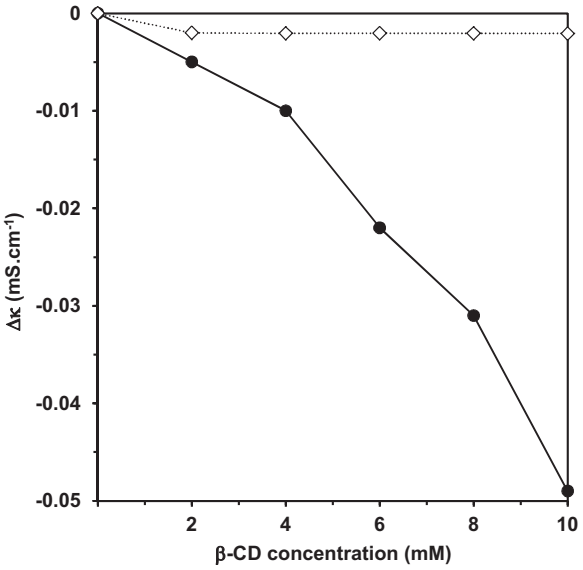

Fig. 2. Variation in conductivity as a function of the concentration of β-CD in 50 mL of deionized water (◊) and in 50 mL of aqueous $Co(NO_3)_2$ with a concentration of 1 mM (●). Δκ was calculated by subtracting the absolute value κ of the corresponding solution from that of the reference solution prepared without β-CD.

3. Results and discussion

3.1. Impregnation solutions

Interactions between β-CD and cobalt nitrate have been initially investigated by UV–vis spectroscopy (Fig. 1). In the visible region, the absorption spectrum of the initial solution of cobalt nitrate (without β-CD; Fig. 1a) exhibits a broad band with a shoulder at λ values of 516 and 470 nm, assignable to the $^4T_{1g}$ (F) → $^4T_{1g}$ (P) and $^4T_{1g}$ (F) → $^2A_{1g}$ (P) transitions of high-spin Co^{2+} ions in octahedral coordination, respectively [53]. We observe that gradual addition in solution of native β-CD to cobalt nitrate causes a slight shift of the absorption maxima towards lower wavelengths, indicating that the coordination environment of cobalt is slightly affected. Thus, at the highest concentration of β-CD, the spectral-blue shift reaches approximately the value of 6 nm (Fig. 1f). The occurrence of the shift can be explained by the fact that the β-CD molecules have the capacity to interfere with the coordination sphere of Co(II) ion through their penetration into the solvation shell. Note that the position of the peak at ca. 300 nm ascribed to the $n \rightarrow \pi^*$ transition in nitrates does not appear to be influenced by the presence of β-CD, suggesting no detectable change in the counter-anion environment of the cobalt complex.

The impact of β-CD on cobalt nitrate in aqueous solutions has further been examined by ion conductivity measurements. Experiments have been performed in the following manner: progressively increasing amounts of β-CD are added to 50 mL of 1 mM cobalt nitrate hexahydrate solution and plots of conductivity of the so-obtained solutions are reported in the steady-state in Fig. 2. For comparison, the conductivity of solutions of β-CD with increasing concentrations has also been determined. Whereas no marked change in the conductivity is noticed upon increasing the amount of β-CD in water, it is readily apparent that the conductivity of $Co(NO_3)_2$ is strongly affected by β-CD. Clearly, the conductivity drops gradually with increasing β-CD loading. This effect can be explained by the fact that the movement of the mobile ions, i.e. Co^{2+} and NO_3^- becomes increasingly hindered in the presence of the oligosaccharide, as a result of the mutual interactions between the β-CD and the cobalt salt.

Complementary information has been obtained by means of DLS measurements. Fig. 3 gives the size distributions for a 1 mM β-CD solution and a mixture of 1 mM β-CD with 1 mM $Co(NO_3)_2$. When no cobalt nitrate is added to β-CD, the size distribution curve reveals a bimodal distribution. The first mode is ascribed to the monomeric β-CD (1.5 nm) whereas the second is attributable to aggregates of cyclodextrin (140 nm). It must be specified that, in pure aqueous solutions, native cyclodextrins (α-CD, γ-CD and especially β-CD) have a strong tendency to self-associate through hydrogen bonding and form large aggregates of a few hundred of nanometers [54–56].

As clearly shown in Fig. 3, the aggregation state of β-CD is deeply disturbed by the addition of cobalt nitrate. Indeed, the band characteristic of the largest CD aggregates has completely disappeared after two hours stirring (as mentioned in the Section 2.2, the solutions are kept under stirring for 2 h before DLS analysis). Consequently, a monomodal population is observed, yielding a mean hydrodynamic diameter of 2.3 nm with 80% between 1.5

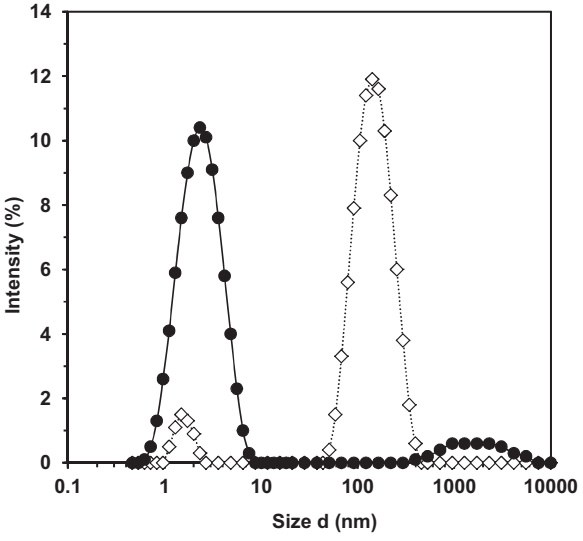

Fig. 3. Size distributions obtained by DLS measurements performed on an aqueous solution of β-CD at the concentration of 1 mM (◊) and on the mixture of β-CD and $Co(NO_3)_2$ at the same concentrations of 1 mM (●).

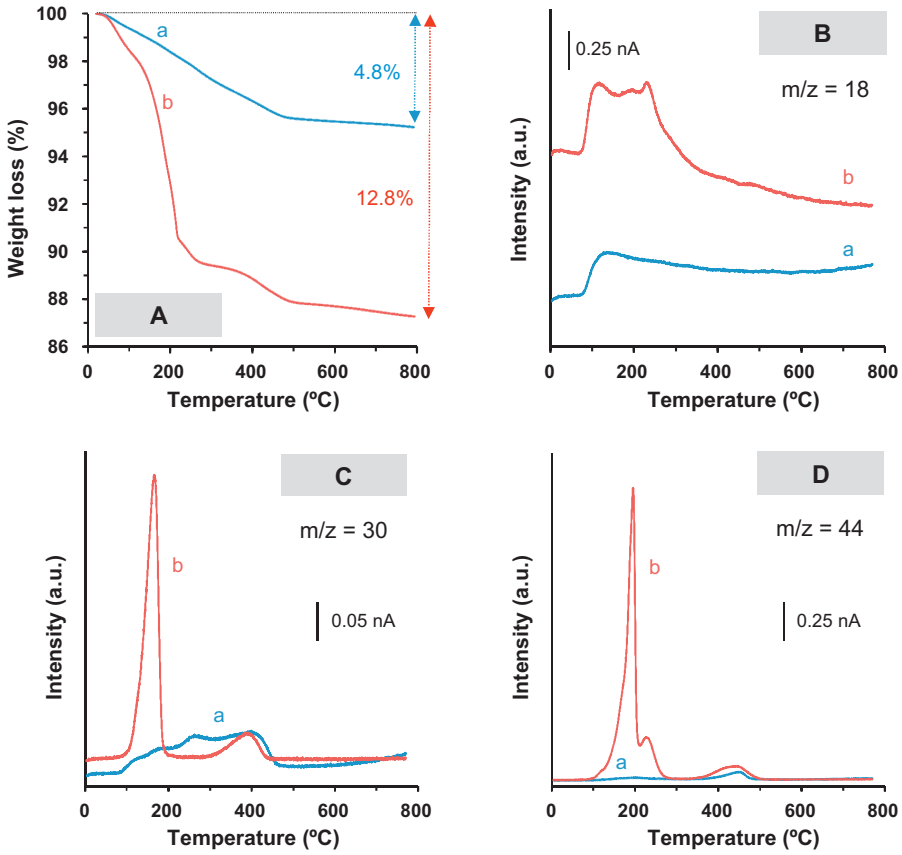

Fig. 4. Thermograms (A) and mass fragmentograms of *m*/*z* 18 (B), *m*/*z* 30 (C) and *m*/*z* 44 (D) in the TG–MS analysis performed on the following dried samples: Co(N)/Zr (a) and Co-$CD_{0.01}$/Zr (b).

and 5 nm, as a result of the formation of monomeric units or small oligomeric assemblies of β-CD. These changes suggest that the weak intermolecular H-bonds that bind cyclodextrins together can be simply disrupted by insertion of cobalt nitrate, thereby modifying the attractive forces between neighboring cyclodextrin molecules. Accordingly, when $Co(NO_3)_2$ is dissolved in the aqueous solution of β-CD, it is proposed that the cobalt ionic species are chelated to hydroxyls groups located at the rim of the cavity.

Finally, the above results have provided evidence for the occurrence of molecule-ion interactions in solution between $Co(NO_3)_2$ and β-CD. These features can be related to the fact that β-CD has a chelating capacity to cobalt atoms thanks to its large number of hydroxyl groups present on the external face of the torus.

3.2. Dried oxide solids

The ability of cyclodextrin to interact with cobalt nitrate has further been used to prepare a series of ZrO_2 supported-cobalt oxide solids (5 wt.% Co) with impregnating solutions having different ratios of cobalt to β-CD. Thus, evidence of the impact of β-CD to retard the formation of the cobalt oxide phase has been shown by thermogravimetric analysis coupled to mass spectroscopy (Fig. 4). The analysis has been carried out on the following samples: Co(N)/Zr and Co-$CD_{0.01}$/Zr, the latter, with its low β-CD content, has been selected to restrict overheating during the decomposition of the precursor. For the dried solid prepared without using β-CD, we observe a slow and continuous weight loss of ca. 4.8% in the whole temperature range (Fig. 4a). The mass spectrometry signal of H_2O (*m*/*z* = 18; Fig. 4b) and NO (*m*/*z* = 30; Fig. 4c) suggests that, after an initial minor weight loss of about 0.8% at a temperature below 120 °C mainly due to the release of adsorbed water, the major weight loss of about 4.0% is associated to the decomposition of the nitrate salt. Note that the weight loss is considerably lower than that could be expected by considering the total conversion of fully hydrated $Co(NO_3)_2{\cdot}6H_2O$ into Co_3O_4 (14.1%). The discrepancy can be explained by the fact that part of the nitrate and part of the water molecules from the cobalt hydrate shell have already been released during the drying (100 °C, overnight), responsible for the rapid formation of the cobalt oxide phase.

In contrast, the Co-$CD_{0.01}$/Zr exhibits a more complex thermal behavior with at least three distinct weight losses. The most significant weight loss, which occurs between 150 and 300 °C, is mainly attributable to the thermal degradation of β-CD accompanied by the simultaneous formation of H_2O and CO_2 (*m*/*z* = 44; Fig. 4d). The other two weight losses observed in the ranges 80–200 °C and 300–500 °C are dominated by the release of NO produced by the decomposition of nitrate. Notably, the TG–MS analysis reveals that the addition of β-CD to the cobalt precursor has a large influence on the thermal stability of the nitrate species, especially in the low-temperature region. Indeed, it is readily apparent that a large amount of NO is suddenly released by the degradation of the β-CD-modified cobalt precursor at about 160 °C. This result differs from that previously observed with the control sample, where only a low-intense signal of NO was detected. Indeed, the use of β-CD retards the thermal decomposition of nitrates and therefore that of the cyclodextrin-cobalt nitrate adducts, thus minimizing the aggregation process by preventing the interactions of cobalt ions together. Finally, the total weight loss is of 12.8%. This value, which is relatively close to the theoretical loss of 14.9%, is a further evidence of the preservation of the β-CD-Co(II) precursor after the drying cycle without the formation of cobalt oxide phase.

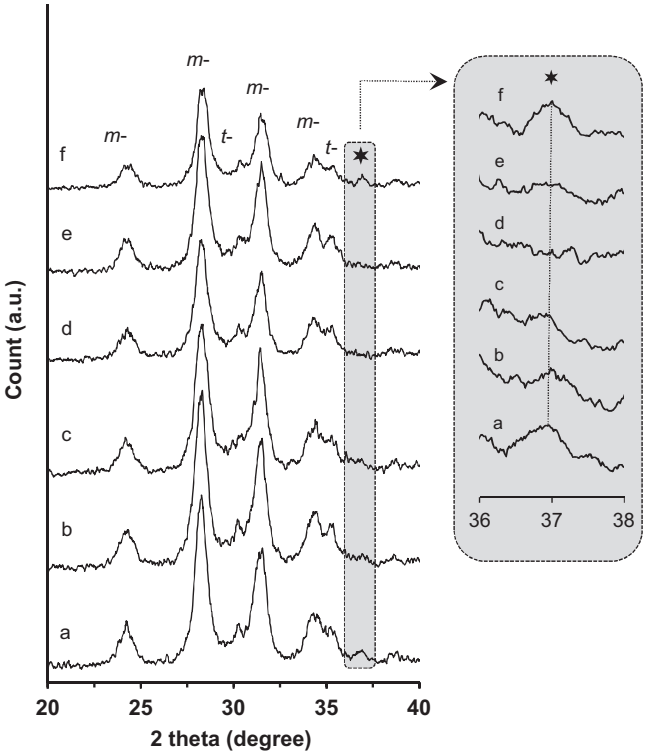

Fig. 5. XRD patterns of the calcined catalysts: (a) Co(N)/Zr, (b) Co-$CD_{0.01}$/Zr, (c) Co-$CD_{0.05}$/Zr, (d) Co-$CD_{0.1}$/Zr, (e) Co-$CD_{0.2}$/Zr and (f) Co-CD_1/Zr. *m*- and *t*- indicate the monoclinic and tetragonal phase, respectively. The diffraction peak marked with an asterisk is indexed to the pure fcc Co_3O_4 structure (JCPDS No. 42-1467).

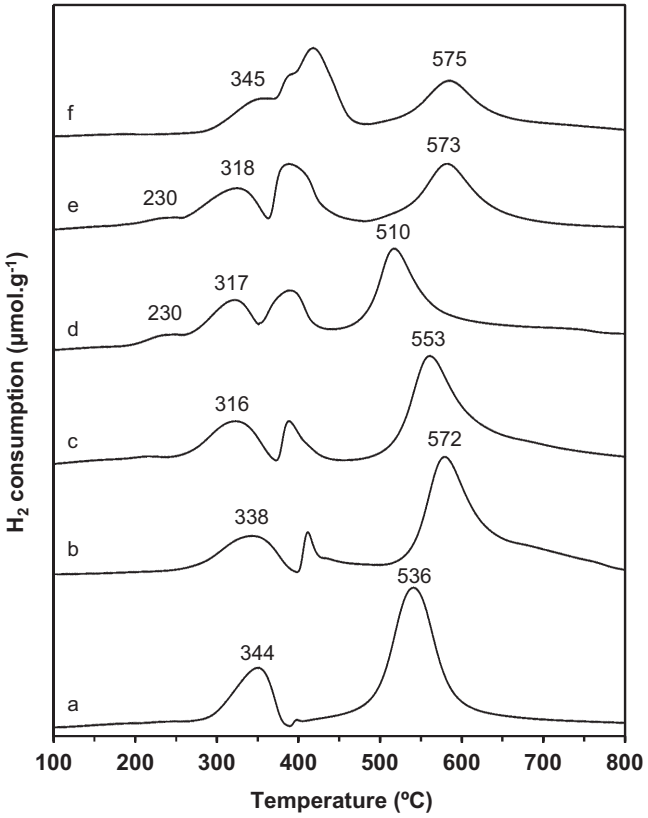

Fig. 6. H_2-TPR profiles of the calcined catalysts: (a) Co(N)/Zr, (b) Co-$CD_{0.01}$/Zr, (c) Co-$CD_{0.05}$/Zr, (d) Co-$CD_{0.1}$/Zr, (e) Co-$CD_{0.2}$/Zr and (f) Co-CD_1/Zr.

Further spectroscopic evidence of the impact of β-CD to retard the formation of the cobalt oxide phase has been also been shown by Diffuse Reflectance UV–vis spectrometry. Indeed, the DRUV-Vis spectrum of control Co(N)/Zr shows the presence of Co_3O_4 phase generated by the low-temperature hydrolysis of cobalt nitrate, with bands peaking at ca. 460 and 710 nm ascribed to the mixed-valence cobalt oxide [$Co^{III}_2Co^{II}O_4$] [57,58]. When the catalysts are prepared in the presence of β-CD, the spectra exhibit absorption bands at ca. 340 and 515 nm, which can be viewed as an evidence of the presence of isolated octahedral Co(II) ions after their deposit on zirconia (Fig. S1 in the supporting information).

3.3. Calcined oxide catalysts

The catalysts have been further investigated by XRD after calcination and the patterns are given in Fig. 5. The prominent XRD lines at $2\theta = 28.2^\circ$, 33.2° and 31.5° indicates that the zirconia support mainly consists of the monoclinic form with a small proportion of tetragonal phase (<15 wt.%). Without addition of β-CD to the cobalt precursor, the XRD pattern of the control Co(N)/Zr shows the presence of a weak reflection peak at $2\theta = 36.8^\circ$ ascribed to the face-centered cubic Co_3O_4 structure (Fig. 5a). This observation is not surprising given that the Co_3O_4 phase was already detectable in the DRUV-Vis spectrum of the sample after drying. In contrast, addition of sub-stoichiometric amounts of β-CD to cobalt causes a decrease in the intensity and broadening of the Co_3O_4 reflections (Fig. 5b–e). This effect is particularly noticeable when the ratio of β-CD to Co reaches the value of 0.1 (see the inset of Fig. 5). This tendency is in line with the previous characterization carried out on the dried solids showing that the proportion of cobalt oxide decreased with β-CD addition and supports the view of a beneficial contribution of β-CD on the cobalt dispersion in the final structure of the catalysts. Indeed, the broadening of cobalt oxide reflection in the XRD patterns implies that the cobalt species are more finely dispersed on the surface of zirconia, in the form of amorphous and/or nanocrystalline particles. This result could be correlated to the above-mentioned stabilization of β-CD-Co(II) adducts on the zirconia support, preserving the dispersion of the cobalt species by delaying the formation, growth and aggregation of cobalt oxide particles.

However, this result cannot be generalized to all ratios of β-CD to cobalt. As clearly evidenced by the XRD pattern of Co-CD_1/Zr (Fig. 5f), an increase in the relative amount of β-CD to the impregnating solution again leads to reappearance of large Co_3O_4 crystallites after calcination. This observation can be connected with the fact that, when a high content of oligosaccharide additive is used, the risk of over-oxidation during the heating treatment is enhanced, with formation of hot-spots and heat transfer limitations due to the exothermicity of β-CD decomposition reaction. Indeed as described in the Section 2.1, the catalysts are subjected to a calcination step under air at 400 °C for 4 h to ensure the total decomposition of the organic content. Note that the efficiency of the β-CD removal during calcination has been supported by nitrogen adsorption/desorption measurements. The data before and after the thermal treatment are reported in Table 1 and clearly show that the specific surface area is almost recovered by the oxidation treatment (for instance, 56.3 $m^2\ g^{-1}$ for Co-$CD_{0.1}$/Zr vs 56.6 $m^2\ g^{-1}$ for Co(N)/Zr).

3.4. Catalysts reducibility studied by temperature programmed reduction

Cobalt reducibility of zirconia supported-cobalt catalysts has been estimated from H_2-TPR measurements. Fig. 6 shows the TPR profiles while Table 1 lists the resulting data in terms of hydrogen consumption and reduction temperatures.

As shown in Fig. 6a, the shape of the TPR profile of Co(N)/Zr exhibits two distinct hydrogen consumptions in a low and high temperature region, corresponding to two different reducible cobalt species or cobalt reduction steps. The first hydrogen consumption occurring at 344 °C is assigned to the transformation of Co^{3+} to Co^{2+} (Eq. (1)) whereas the second one at 536 °C is associated with the reduction of Co^{2+} to zerovalent cobalt (Eq. (2)). In a quantitative point of view, the first hydrogen consumption is about 23% of the total uptake. Notably, this value is close to the theoretical expected value of 25%, confirming that the low-temperature consumption is attributable to the reduction of Co^{3+} ions within the Co_3O_4 phase [28]. More generally it is worth mentioning that, for all investigated samples, very good correlations between the theoretical and experimental total H_2 consumptions could have been established, with discrepancies ranging from 0 to 3% (Table 1). These data are consistent with the fact that all Co_3O_4 species are fully reduced to metallic cobalt at the end of the H_2-TPR experiment and that Co_3O_4 is the dominant cobalt component stabilized on all air-calcined samples. The formation of stable mixed Co-Zr oxide phases, with hard-to-reduce cobalt species, can therefore be excluded [59].

$$Co_3O_4 + H_2 \rightarrow 3CoO + H_2O \quad (1)$$

$$3CoO + 3H_2 \rightarrow 3Co + 3H_2O \quad (2)$$

However, when examining in more detail the Co-CD_x/Zr samples, the TPR profiles show that the cyclodextrin-assisted impregnation method affects the reducibility of the cobalt oxide species. Indeed, addition of β-CD at sub-stoichiometric ratios is accompanied by a shift of the first peak towards lower temperatures (338–318 °C with increasing x from 0.01 to 0.2) and in some cases by the appearance of a shoulder at about 230 °C (x = 0.1 and 0.2). This suggests that the addition of β-CD promotes the formation of cobalt sites with enhanced reducibility. The H_2 consumption in this low-temperature region (estimated by peak deconvolution) represents 22–23% of the total consumption, suggesting that only Co^{3+} to Co^{2+} reduction is involved here. In addition, the subsequent conversion of CoO to cobalt metal appears also to be very sensitive to the size and/or morphology of Co_3O_4 [60]. Interestingly, a peak is observed at temperatures close to 400 °C and its contribution seems to be highly dependent on the initial content of β-CD; the higher amount of β-CD, the larger the surface area. This peak can be the result of the subsequent reduction of CoO to Co of the most easily reducible cobalt species formed when cyclodextrin is added in the impregnating solution. Note that this peak is already present in the control sample but its surface area remains extremely small (~1%).

The higher temperature peak (at 536 °C for Co(N)/Zr) relevant to the reaction of CoO to metallic cobalt shift to higher temperatures with addition of cyclodextrin (except for Co-$CD_{0.1}$/Zr). These results may indicate that the second reduction step of CoO to Co is also sensitive to the structure of the cobalt catalysts. It can be suggested that the presence of the metallic cobalt species influence by hydrogen spillover the reduction of the cobalt oxide clusters located in the proximity of the cobalt particles and thus significantly affect the total reducibility of the Co/ZrO_2 catalysts. Notably, this effect would be much more pronounced for Co-$CD_{0.1}$/Zr since the TPR profile shows that complete reduction of cobalt species is achieved more rapidly than with the other samples, with a final reduction step centered at ca. 510 °C. Conversely, in the case of Co-CD_1/Zr, the reduction peaks of the cobalt oxide species are completely repositioned, with reduction features shifted this time towards higher temperatures. At the highest ratio of β-CD to cobalt of 1, the dried oxide solid is more prone to form local hot spots during calcination and produce cobalt oxide aggregates large enough to be detected by XRD as previously observed.

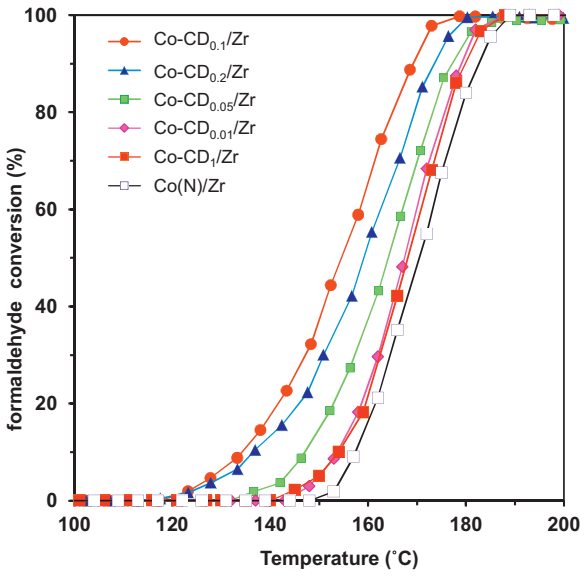

Fig. 7. Temperature dependence of HCHO conversion over zirconia supported-cobalt calcined catalysts. HCHO = 150 ppm, O_2 = 20 vol.%, He balance, Total flow rate = 100 mL min^{-1}, Heating rate of 1 °C min^{-1}.

Finally, according to the data discussed above (DRUV-Vis, TG–MS, XRD and H_2-TPR), it appears that the impregnation method employing mixtures of β-CD and cobalt nitrate in sub-stoichiometric conditions, especially at the ratio of 0.1, is effective in preserving a low degree of crystallinity of cobalt oxide particles while enhancing the redox properties known to have a large influence on the catalytic oxidation activity.

3.5. Catalytic performance in oxidation of formaldehyde

The catalytic properties of the above cobalt-supported zirconia solids have been evaluated in the total oxidation of formaldehyde carried out in the temperature range 25–250 °C and atmospheric pressure. Plots of the conversion of HCHO as a function of the reaction temperature are reported in Fig. 7.

In all cases, the sigmoidal shape of the conversion vs temperature plot is due to the heat generated by the exothermic nature of the oxidation reaction. This leads to a temperature increase which in turn accelerates until total conversion of formaldehyde is achieved, at temperatures below 190 °C. When comparing the light-off temperatures, denoted as T_{50} (temperatures at which 50% of HCHO is converted), it is found that the cobalt-supported catalysts prepared from β-CD appear to be more efficient than the reference Co(N)/Zr catalyst. It is worth adding that, whatever the sample and the temperature, carbon monoxide is not produced, the only reaction products being carbon dioxide and water. This behavior can be easily associated with the ability of Co_3O_4 to promote the oxidation of CO into CO_2 [61,62].

Moreover, the results show that the promoting effect of β-CD is quite dependent on the amount of cyclodextrin used, as illustrated in Fig. 8. The following sequence of T_{50} can be established: Co-$CD_{0.1}$/Zr, 155 °C < Co-$CD_{0.2}$/Zr, 159 °C < Co-$CD_{0.05}$/Zr, 164 °C < Co-$CD_{0.01}$/Zr, 167 °C ~ Co-CD_1/Zr, 168 °C < Co(N)/Zr, 170 °C. Thus, the highest activity (the lowest T_{50}) is obtained for the ratio of β-CD to cobalt of 0.1, resulting in a drop in light-off temperature of 15 °C. It can also be noted that this tendency for the oxidation of formaldehyde oxidation is valid at low conversion (T_{20}) and high conversion (T_{90}). Finally, reproducibility of the catalyst preparation was checked with the best ratio of 0.1, using

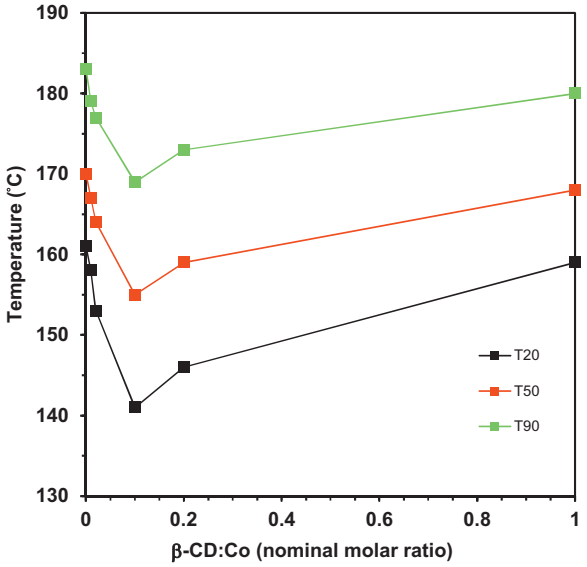

Fig. 8. Temperatures of 20%, 50% and 90% of formaldehyde conversion vs. the nominal molar ratio of β-CD to cobalt in zirconia supported-cobalt calcined catalysts. HCHO = 150 ppm, O_2 = 20 vol.%, He balance, Total flow rate = 100 mL min^{-1}, Heating rate of 1 °C min^{-1}.

two different Co-$CD_{0.1}$/Zr catalysts obtained from two synthesis batches. The deviation of the light-off temperature was less than 2 °C.

Two main factors can account for the best efficiency of Co-$CD_{0.1}$/Zr, namely the presence of small particle size of cobalt oxide with a good surface dispersion and the enhanced reducibility of the cobalt. It can be suggested that the initial ratio of β-CD to cobalt of 0.1 provides optimal conditions for yielding molecule-ion associations between β-CD and $Co(NO_3)_2$ in solution and in the dried solid states after impregnation on the support. Indeed, the starting interactions taking place between β-CD and the metal precursor are known to be of fundamental importance to control the nucleation and growing processes of metal oxide species. In our case, the possibility of forming supramolecular adducts based on β-CD has been evidenced by means of several techniques (UV–vis spectroscopy, conductivity, DLS and TG–MS) and the occurrence of such a phenomenon is usually related to a weakening of the strength of the ionic bonds of the salts caused by molecule–ion interactions [45,46]. Knowing that native β-CD is a polyhydroxylated molecule containing 21 hydroxyl groups, the optimal effect obtained at the ratio of 0.1 (in other words, 2.1 OH groups per cobalt atom) can be rationalized by invoking the formation of supramolecular adduct of Co^{2+} with β-CD, in which the cobalt center would be coordinated by two O atoms from β-CD. In addition, the rigidity and steric hindrance of the cyclodextrin, caused by the cyclic arrangement of the seven glucose units, can also play a critical role. This idea has been supported by an additional catalytic experiment carried out on another control Co_3O_4/ZrO_2 catalyst (5 wt.% Co) promoted by the addition of glucose. This catalyst, denoted as Co-$GL_{0.7}$/Zr, was prepared using exactly the same procedure as that described in the experimental section, except that β-CD (0.1 equiv per cobalt atom) was replaced by methyl-α-D-glucopyranoside (0.7 equiv per cobalt atom), the constitutive building blocks of cyclodextrins. When Co-$GL_{0.7}$/Zr was exposed to formaldehyde oxidation, we have observed that the reaction proceeded much more slowly, achieving 50% conversion at a temperature of 23 °C higher than that of Co-$CD_{0.1}$/Zr (T_{50} = 178 °C and 155 °C, respectively). This example indicates that the presence of hydroxyl groups on isolated glucose rings is not sufficient to provide effective molecule-ion interactions with cobalt ions, thus highlighting the results obtained with β-CD.

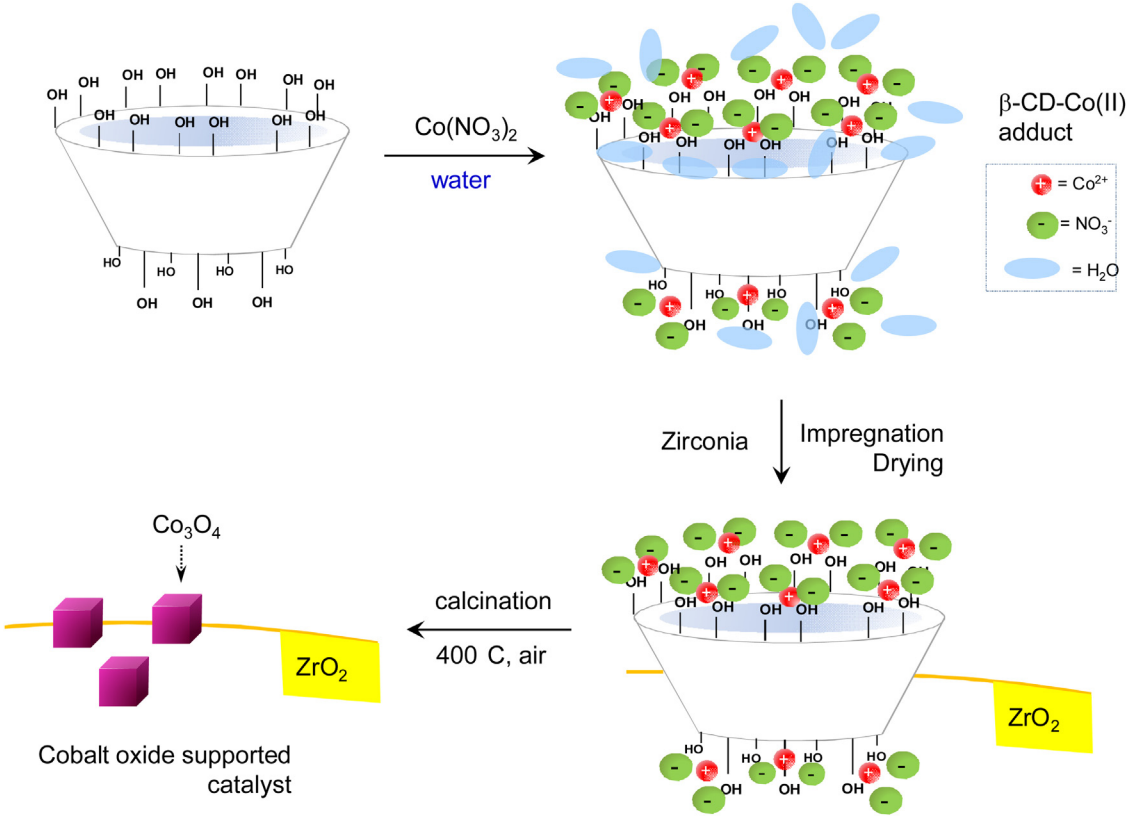

Scheme 2. Schematic illustration of the formation of cobalt oxide particles through the stabilization of β-CD-Co(II) adducts.

Finally, even though molecule-ion interactions via the hydroxyl groups of β-CD and cobalt ions are weak by nature, they allow providing a new environment for the cobalt ions. As illustrated in Scheme 2, β-cyclodextrin can be considered as a scaffold molecule that concentrates the cobalt ions at its close vicinity and leads to the formation of more stable complexes of cobalt ions with β-CD and its oxidation products formed during calcination. This effect affects the rate of cobalt oxide nucleation and results in a higher dispersion and reducibility of Co_3O_4 species, especially at the ratio of β-CD to Co of 0.1. Below the optimal value of 0.1, the decrease in activity may reflect a reduced proportion of β-CD-Co(II) adducts in the impregnating solution at the expense of that of uncomplexed cobalt species. At a ratio higher than 0.1, the excess of free β-CD may lead to high rates of decomposition of the cobalt precursor, due to the exothermicity of the reaction, and therefore to hard-to-control degrees of cobalt agglomeration.

4. Conclusion

In conclusion, we have investigated the possibility of using β-cyclodextrin for preparing by wet impregnation a novel series of zirconia cobalt-supported catalysts for the complete oxidation of formaldehyde. Our data have revealed that the controlled addition of β-CD to cobalt nitrate in the impregnation solution has a strong impact on the final structure of the catalysts, in terms of reducibility and dispersion of active species. The phenomenon has been related to the fact that the association of β-CD and $Co(NO_3)_2$ could give rise to the formation of supramolecular adducts. This association occurs first in the impregnating solution. The thermal oxidative treatments (drying, calcination) of the catalyst containing cyclodextrin results in a formation of more stable complexes of cobalt ions with cyclodextrins and products of cyclodextrin mild oxidation. This hypothesis has been supported on the one hand, in solution by UV–vis spectroscopy, ion conductivity and DLS measurements, and on the other hand, in the dried state after impregnation on the support by DRUV and TG–MS analysis. These complexes minimize the aggregation process by preventing the interactions of cobalt ions together and their subsequent decomposition results in the formation of smaller and more reducible cobalt oxide particles on zirconia. However, the molar ratio of β-CD to cobalt appears to be the key factor, the ratio of 0.1 leading to the most significant effects. Indeed, the optimization of the catalyst preparation shows that the Co-$CD_{0.1}$/Zr sample affords the highest activity for the oxidation of formaldehyde.

Acknowledgments

Lei Bai is grateful to the China Scholarship Council (CSC) for the PhD grant support (Grant No 2010634110). The laboratory participates in the Institut de Recherche en ENvironnement Industriel (IRENI), which is financed by the Communauté Urbaine de Dunkerque, the Région Nord Pas-de-Calais, the Ministère de l'Enseignement Supérieur et de la Recherche, the CNRS and European Regional Development Fund (ERDF). The authors are grateful to Olivier Gardoll (UCCS, University of Lille, France) for the TG–MS and TPR analyses. The authors are grateful to Roquette Frères (Lestrem, France) for the generous gift of cyclodextrins.

Appendix A. Supplementary data

Supplementary data associated with this article can be found, in the online version, at http://dx.doi.org/10.1016/j.apcatb.2013.03.015.

References

[1] R.G. Derwent, in: R.E. Hester, R.M. Harrison (Eds.), Volatile Organic Compound in the Atmosphere, Issues in Environmental Science and Technology N°4, RSC, Cambridge, 1995, pp. 1–15.
[2] Environmental Fact Sheet No. 19, January 2006, Produced by The Swedish NGO Secretariat on Acid Rain, Göteborg, Sweden.
[3] X.S. Zhao, Q. Ma, G.Q.M. Lu, Energy and Fuels 12 (1998) 1051–1054.
[4] B.K. Min, C.M. Friend, Chemical Reviews 107 (2007) 2709–2724.
[5] V.P. Santosa, S.A.C. Carabineiro, P.B. Tavares, M.F.R. Pereira, J.J.M. Órfão, J.L. Figueiredoa, Applied Catalysis B: Environmental 99 (2010) 198–205.
[6] L.F. Liotta, Applied Catalysis B: Environmental 100 (2010) 403–412.
[7] W.B. Li, J.X. Wang, H. Gong, Catalysis Today 148 (2009) 81–87.
[8] J. Gutiérrez-Ortiz, B. de Rivas, R. López-Fonseca, J.R. González-Velasco, Applied Catalysis B: Environmental 65 (2006) 191–200.
[9] M. Alifanti, M. Florea, V.I. Pârvulescu, Applied Catalysis B: Environmental 70 (2007) 400–405.
[10] M. Labaki, J.F. Lamonier, S. Siffert, E.A. Zhilinskaya, A. Aboukaïs, Colloids and Surfaces A: Physicochemical and Engineering Aspects 227 (2003) 63–75.
[11] M. Labaki, J.F. Lamonier, S. Siffert, E.A. Zhilinskaya, A. Aboukaïs, Applied Catalysis B: Environmental 43 (2003) 261–271.
[12] C. Cellier, V. Ruaux, C. Lahousse, P. Grange, E.M. Gaigneaux, Catalysis Today 117 (2006) 350–355.
[13] V. Iablokov, K. Frey, O. Geszti, N. Kruse, Catalysis Letters 134 (2010) 210–216.
[14] M.A. Sidheswarana, H. Destaillats, D.P. Sullivan, J. Larsen, W.J. Fiska, Applied Catalysis B: Environmental 107 (2011) 34–41.
[15] Y.-F. Yu Yao, Journal of Catalysis 33 (1974) 108–122.
[16] P. Thormählen, M. Skoglundh, E. Fridell, B. Andersson, Journal of Catalysis 188 (1999) 300–310.
[17] J. Jansson, A.E.C. Palmqvist, E. Fridell, M. Skoglundh, L. Österlund, P. Thormählen, V. Langer, Journal of Catalysis 211 (2002) 387–397.
[18] S. Sun, Q. Gao, H. Wang, J. Zhu, H. Guo, Applied Catalysis B: Environmental 97 (2010) 284–291.
[19] K. Schmidt, K. Szałowski, J. Krawczyk, Petryk, Applied Catalysis A-General 175 (1998) 147–157.
[20] L.F. Liotta, M. Ousmane, G. Di Carlo, G. Pantaleo, G. Deganello, G. Marci, L. Retailleau, A. Giroir-Fendler, Applied Catalysis A-General 347 (2008) 81–88.
[21] Y. Xie, F. Dong, S. Heinbuch, J.J. Roca, E.R. Bernstein, Physical Chemistry Chemical Physics 12 (2010) 947–959.
[22] Y.M. Yang, B.Z. Wan, Applied Catalysis A-General 114 (1994) 35–49.
[23] R.S. Drago, K. Jurczyk, D.L. Singh, V. Young, Applied Catalysis B: Environmental 6 (1995) 155–168.
[24] Z. Zhao, X.L. Lina, R. Jin, G. Wang, T. Muhammad, Applied Catalysis B: Environmental 115–116 (2012) 53–62.
[25] L.A. Boot, H.J.V. Meike, H.J.V. Kerkhoffs, B.Th. Van Der Linden, A.J. Van Dillen, J.W. Geus, F.R. Van Buren, Applied Catalysis A 137 (1996) 69–86.
[26] J. van de Loosdrecht, M. van der Haar, A.M. van der Kraan, A.J. van Dillen, J.W. Geus, Applied Catalysis A-General 150 (1997) 365–376.
[27] M. Kraum, M. Baerns, Applied Catalysis A-General 186 (1999) 189–200.
[28] F. Wyrwalski, J.F. Lamonier, S. Siffert, A. Aboukaïs, Applied Catalysis B: Environmental 70 (2007) 393–399.
[29] F. Wyrwalski, J.F. Lamonier, S. Siffert, L. Gengembre, A. Aboukaïs, Catalysis Today 119 (2007) 332–337.
[30] F. Wyrwalski, J.F. Lamonier, M. Perez-Zurita, S. Siffert, A. Aboukaïs, Catalysis Letters 108 (2006) 87–95.
[31] F. Wyrwalski, J.M. Giraudon, J.F. Lamonier, Catalysis Letters 137 (2010) 141–149.
[32] J.S. Girardon, E. Quinet, A. Griboval-Constant, P.A. Chernavskii, L. Gengembre, A.Y. Khodakov, Journal of Catalysis 248 (2007) 143–157.
[33] A. Jean-Marie, A. Griboval-Constant, A.Y. Khodakov, F. Diehl, Catalysis Today 171 (2011) 180–185.
[34] J. Hong, E. Marceau, A.Y. Khodakov, A. Griboval-Constant, C. La Fontaine, F. Villain, V. Briois, P.A. Chernavskii, Catalysis Today 175 (2011) 528–533.
[35] A. Denicourt-Nowicki, A. Roucoux, F. Wyrwalski, E. Monflier, A. Ponchel, Chemistry-A European Journal 14 (2008) 8090–8093.
[36] F. Wyrwalski, B. Léger, C. Lancelot, A. Roucoux, E. Monflier, A. Ponchel, Applied Catalysis A-General 391 (2011) 334–341.
[37] L.X. Song, M. Wang, Z. Dang, F.Y. Yun Du, Journal of Physical Chemistry B 114 (2010) 3404–3410.
[38] J. Yang, L.X. Song, J. Yang, Z. Dang, J. Chen, Dalton Transactions 41 (2012) 2393–2398.
[39] J. Szejtli, Chemical Review 98 (1998) 1743–1753.
[40] M.V. Rekharsky, Y. Inoue, Chemical Review 98 (1998) 1875–1917.
[41] H. Bricout, F. Hapiot, A. Ponchel, S. Tilloy, E. Monflier, Current Organic Chemistry 14 (2010) 1296–1307.
[42] F. Hapiot, A. Ponchel, S. Tilloy, E. Monflier, Comptes Rendus Chimie 14 (2011) 149–166.
[43] A. Nowicki-Denicourt, A. Ponchel, E. Monflier, A. Roucoux, Journal of Chemical Society, Dalton Transactions (2007) 5714–5719.
[44] E. Norkus, Journal of Inclusion Phenomena and Macrocyclic Chemistry 65 (2009) 237–248.
[45] S.Z. Pan, L.X. Song, L. Bai, M. Wang, J.H. Zhu, J. Chen, Current Organic Chemistry 15 (2011) 862–868.
[46] L.X. Song, S.Z. Pan, L. Bai, Z. Dang, M. Wang, F.Y. Du, J. Chen, Supramolecular Chemistry 23 (2011) 447–454.

[47] A. Jean-Marie, A. Griboval-Constant, A.Y. Khodakov, E. Monflier, F. Diehl, Chemical Communications 47 (2011) 10767–10769.
[48] A.Y. Khodakov, W. Chu, P. Fongarland, Chemical Review 107 (2007) 1692–1744.
[49] K.H. Kim, S.A. Jahan, J.T. Lee, Journal of Environmental Science and Health. Part C, Environmental Carcinogenesis and Ecotoxicology Reviews 29 (2011) 277–299.
[50] D.A.M. Monti, A. Baiker, Journal of Catalysis 83 (1983) 323–335.
[51] B. Jouguet, A. Gervasini, A. Auroux, Chemical Engineering and Technology 18 (1995) 243–247.
[52] P. Malet, A. Caballero, Journal of the Chemical Society, Faraday Transactions 1 (84) (1988) 2369–2375.
[53] Y. Okamoto, K. Nagata, T. Adachi, T. Imanaka, K. Inamura, T. Takyu, Journal of Physical Chemistry 95 (1991) 310–319.
[54] A.W. Coleman, I. Nicolis, N. Keller, J.P. Dalbiez, Journal of Inclusion Phenomena and Molecular Recognition Chemistry 13 (1992) 139–143.
[55] G. González-Gaitano, P. Rodríguez, J.R. Isasi, M. Fuentes, G. Tardajos, M. Sánchez, Journal of Inclusion Phenomena and Molecular Recognition Chemistry 44 (2002) 101–105.
[56] R. Herbois, S. Noël, B. Léger, L. Bai, A. Roucoux, E. Monflier, A. Ponchel, Chemical Communications 48 (2012) 3451–3453.
[57] A.A. Verberckmoes, B.M. Weckhuysen, R.A. Schoonheydt, Microporous and Mesoporous Materials 22 (1998) 165–178.
[58] M. Zayat, D. Levy, Chemistry of Materials 12 (2000) 2763–2769.
[59] V.G. Milt, E.A. Lombardo, M.A. Ulla, Applied Catalysis B: Environmental 37 (2002) 63–73.
[60] X. Xie, W. Shen, Nanoscale 1 (2009) 50–60.
[61] Z. Zhao, M.M. Yung, U.S. Ozkan, Catalysis Communications 9 (2008) 1465–1471.
[62] M.M. Yung, Z. Zhao, M.P. Woods, U.S. Ozkan, Journal of Molecular Catalysis A: Chemical 279 (2008) 1–9.